Published in final edited form as:
Dev Biol. 2014 August 15; 392(2): 245–255. doi:10.1016/j.ydbio.2014.05.020.

Functional characterization of Prickle2 and BBS7 identify overlapping phenotypes yet distinct mechanisms

Xue Mei[1], **Trudi A. Westfall**[1], **Qihong Zhang**[2,3], **Val C. Sheffield**[2,3], **Alexander G. Bassuk**[2], and **Diane C. Slusarski**[1,*]

[1]Department of Biology, University of Iowa, Iowa City, Iowa 52242, USA

[2]Department of Pediatrics, University of Iowa Carver College of Medicine, Iowa City, Iowa 52242, USA

[3]Howard Hughes Medical Institute, University of Iowa Carver College of Medicine, Iowa City, Iowa 52242, USA

Abstract

Ciliopathies are genetic disorders that are caused by dysfunctional cilia and affect multiple organs. One type of ciliopathy, Bardet-Biedl Syndrome, is a rare disorder characterized by obesity, retinitis pigmentosa, polydactyly, mental retardation and susceptibility to cardiovascular diseases. The Wnt/Planar Cell Polarity (PCP) has been associated with cilia function and ciliogenesis in directing the orientation of cilia and basal bodies. Yet the exact relationship between PCP and ciliopathy is not well understood. Here, we examine interactions between a core PCP component, *Prickle2* (*Pk2*), and a central BBS gene, *Bbs7*, using gene knockdown in the zebrafish. *pk2* and *bbs7* knockdown both disrupt the formation of a ciliated organ, the Kupffer's Vesicle (KV), but do not display a synergistic interaction. By measuring cell polarity in the neural tube, we find that *bbs7* activity is not required for *Pk* asymmetric localization. Moreover, BBS protein complex formation is preserved in the *Pk2*-deficient ($Pk2^{-/-}$) mouse. Previously we reported an intracellular melanosome transport delay as a cardinal feature of reduced *bbs* gene activity. We find that *pk2* knockdown suppresses *bbs7*-related retrograde transport delay. Similarly, knockdown of *ift22*, an anterograde intraflagellar transport component, also suppresses the *bbs7*-related retrograde delay. Notably, we find that *pk2* knockdown larvae show a delay in anterograde transport. These data suggest a novel role for Pk2 in directional intracellular transport and our analyses show that PCP and BBS function independently, yet result in overlapping phenotypes when knocked down in zebrafish.

*To whom correspondence should be addressed at: Department of Biology, University of Iowa, 246 Biology Building, Iowa City, IA 52242, USA. Fax 319 335-1069; Phone 319-335-3229; diane-slusarski@uiowa.edu.

COMPETING INTEREST STATEMENT None declared.

AUTHOR CONTRIBUTIONS

D.C.S, Q.Z and X.M conceived and designed the experiments. X.M, T.A.W, D.C.S. and Q.Z performed the experiments. A.G.B contributed to the reagents. D.C.S, Q.Z and X.M analyzed the data. X.M, Q.Z, V.C.S, A.G.B and D.C.S wrote the paper.

Keywords

Planar Cell Polarity; Bardet-Biedl Syndrome; cilia; intracellular transport; zebrafish; Prickle2; Kuppfer's Vesicle; retinal neurogenesis

INTRODUCTION

The cilium is a subcellular organelle that protrudes from the plasma membrane of almost every vertebrate cell. The cilium serves as a sensory organelle for developmental signals or as a motile structure that creates fluid flow (Marshall and Nonaka, 2006; Singla and Reiter, 2006). Dysfunctional cilia underlie a number of human genetic conditions that affect multiple organ systems leading to blindness, heart disease, infertility, obesity or diabetes. One such syndrome, Bardet-Biedl syndrome (BBS), is a rare genetic disorder characterized by obesity, retinitis pigmentosa, polydactyly, mental retardation and susceptibility to cardiovascular diseases (Bardet, 1995; Biedl, 1995; Green et al., 1989). There is considerable interest in understanding the molecular mechanisms involved in BBS as phenotypes associated with this disorder are commonly found within the general population. While ciliopathies can present overlapping phenotypes, the extent to which the pathways mechanistically overlap has yet to be determined.

Phenotypes associated with BBS can be attributed to defects in cilia maintenance and intracellular transport (Blacque and Leroux, 2006). To date, nineteen BBS genes have been reported (Aldahmesh et al., 2014; Scheidecker et al., 2014; Zhang et al., 2014). Seven proteins (BBS1, BBS2, BBS4, BBS5, BBS7, BBS8, BBS9 and BBS18, also known as BBIP10) form a stable complex, the BBSome, which mediates protein trafficking to the ciliary membrane and perhaps to other membrane compartments (Loktev et al., 2008; Nachury et al., 2007). Another BBS protein, BBS3, is a member of the Ras superfamily of small GTPases and controls BBSome recruitment to the membrane and BBSome ciliary entry (Fan et al., 2004; Jin et al., 2010; Pasqualato et al., 2002; Zhang et al., 2011). Three other BBS proteins (BBS6, BBS10, BBS12) form another protein complex with the CCT/TRiC family of group II chaperonins and mediate BBSome assembly (Seo et al., 2010). The discovery that various BBS proteins interact to form complexes (the BBSome and the BBS-chaperonin complex) with critical ciliary function is consistent with the overlapping phenotypes arising from mutations in different BBS genes (Nachury et al., 2007; Seo et al., 2010; Tayeh et al., 2008).

Animal models have provided important mechanistic advances in understanding the role of BBS proteins. In the zebrafish, there have been two hallmark phenotypes consistently found with knockdown of all BBS genes tested to date: a reduced or absent Kupffer's vesicle (KV), a ciliated structure that is involved in proper left-right patterning of organs, and delayed intracellular transport (Baye et al., 2011; Pretorius et al., 2010; Seo et al., 2010; Tayeh et al., 2008; Yen et al., 2006). Individual knockdown of some BBS genes have also been reported to lead to CE defects during gastrulation (Gerdes et al., 2007; May-Simera et al., 2010; Ross et al., 2005).

Many developmental pathways are important for cilia formation and function. The Wnt/Planar Cell Polarity (PCP) pathway has been shown to influence cilia orientation and polarity (Montcouquiol et al., 2003; Qian et al., 2007; Wang et al., 2005; Wang et al., 2006). PCP was first described in *Drosophila* as affecting hair cell orientation in the wing and directional cell arrangement in the ommatidia (Jenny et al., 2003; Jenny et al., 2005; Tree et al., 2002). In vertebrates, the PCP pathway regulates cell movement such as convergence and extension (CE) during gastrulation (Roszko et al., 2009). During gastrulation, cells migrate toward the midline lengthening and narrowing the embryos along the anterior-posterior (AP) axis. Defects in PCP components result in CE defects resulting in a shorter AP axis (Roszko et al., 2009). Core PCP components, Dishevelled (Dvl), Prickle (Pk) and Van Gogh (Vangl), have been linked to ciliogenesis and cilia tilting (Borovina et al., 2010; Oteiza et al., 2010; Park et al., 2008). Dvl localizes to basal bodies and promotes protein docking (Hashimoto et al., 2010; Mahuzier et al., 2012; Park et al., 2008; Zilber et al., 2013), while Pk and Vangl regulate cilia length and cilia tilting in the zebrafish KV, respectively (Borovina et al., 2010; Oteiza et al., 2010).

PCP and BBS proteins both affect cilia, however previous studies have generated conflicting interpretations as to the extent to which they act in a common pathway or have distinct roles. The phenotypic overlap between PCP and gene knockdown of some bbs genes in zebrafish suggests an interaction between BBS and PCP (Gerdes et al., 2007; May-Simera et al., 2010; Ross et al., 2005). However, not all the *bbs* genes are involved in CE movements and CE defects are not present in *bbs* hypomorphic genetic mutants (Balciuniene et al., 2013). Additionally, zebrafish and mouse embryos that are mutant for ciliary proteins establish proper planar polarity (Borovina and Ciruna, 2013; Huang and Schier, 2009; Jones et al., 2008). Together these data indicate an indirect interaction between BBS and PCP proteins. CE requires the coordination of many signaling pathways and tissue types, thus measuring CE may not serve as an accurate assessment of gene interaction.

To evaluate functional interaction, we examine phenotypic overlap between BBS and PCP genes in multiple tissue types in the zebrafish. We manipulate *Bbs7* due to its central role as part of the BBSome complex as well as interacting with the BBS-chaperonin complex (Zhang et al., 2012). *Bbs7* mouse knockouts display defects in photoreceptors, brain ependymal cilia and sperm flagella (Zhang et al., 2013). *Pk* is a core component of PCP and modulates CE and neuronal outgrowth (Jiang et al., 2005; Mapp et al., 2011; Mapp et al., 2010; Mei et al., 2013; Ng, 2012; Tada et al., 2003; Takeuchi et al., 2003; Tree et al., 2002; Veeman et al., 2003). Mutation in *PK1* and *PK2* were identified in human epilepsy patients and loss of *pk* also contributes to seizure-like phenotype in mice, flies and zebrafish (Bassuk et al., 2008; Mei et al., 2013; Tao et al., 2011). Mouse *Pk1* is embryonic lethal with polarity defects in the epiblast, but knock out of *Pk2* results in viable animals with slightly smaller body weight and seizure sensitivity (Tao et al., 2012; Tao et al., 2011; Tao et al., 2009).

We analyze shared and individual phenotypes of *bbs7* and *pk2* in the double knockdown zebrafish. We find increased severity of phenotypes in the KV but not a synergistic interaction. While knockdown of both *pk2* and *bbs7* disrupt neural tube polarity, Pk still shows asymmetric localization in *bbs7* knockdown embryos. In addition, BBSome assembly in *Pk2* knockout mice is not altered, suggesting an indirect relationship. We do find that *pk2*

and *bbs7* display opposing activities in intracellular transport. *pk2* knockdown, as well as knockdown of an anterograde transport component are both sufficient to suppress *bbs7*-related transport defects. Moreover, knockdown of *pk2* alters anterograde transport. Our data suggest that *bbs7* and *pk2* act in independent pathways sometimes generating overlapping defects in KV morphogenesis, but distinct phenotypes in the neural tube and in cellular transport of melanosomes. Clarifying the interactions between PCP and BBS provides insight into the normal developmental roles as well as interrogating disease pathophysiology.

MATERIALS AND METHODS

Ethical statement

All the work with zebrafish and mouse is approved by University Animal Care and Use Committee of the University of Iowa.

Mouse *Pk2* mutant

Pk2 knockout mice have been described previously (Tao et al., 2011).

Zebrafish husbandry

Zebrafish adults were maintained under standard conditions and eggs are collected from natural spawnings (Westerfield, 1993). Staging of the embryos was performed according to Kimmel. *et al* (Kimmel et al., 1995).

Morpholinos, expression constructs and primers

pk2 MO: 5′-TGTCCTCCACACTGAAAATAAGAGA-3′, *bbs7* MO : 5′-CAACATGGTTTAGGTTTAACTCCAT-3′ and *ift22* MO: 5′-TCATCGCGGAAAATCACGGCGTTTC-3′ are purchased from Gene Tools, LLC. Amount of MOs delivered into the embryo are as follows: *bbs7* MO: 3.5ng; *ift22* MO: 1ng; *pk2* MO 1.25ng and 2.5ng for KV morphology and retrograde transport assay, 2.5ng for cilia measurements and 4ng for retinal neurogenesis and caffeine assay.

For sequential injections, we inject a group of embryos with one MO at one-cell stage, split the group into two sets, and inject a second MO into one of the sets at two-cell stage. The same needle for this second MO is then used to inject a new set of one-cell stage embryos. The experiment are done in both ways, *pk2* MO first and *bbs7* MO first, to make sure there is no difference with the order of MOs. The same sequential injection strategy was used for RNA injection for the *pk2* IPL rescue and the Centrin-GFP and GFP-Pk localization experiments.

The zebrafish Centrin-GFP construct is a gift from Dr. Caren Norden at The Max Planck Institute of Molecular Cell Biology and Genetics. The GFP-Pk construct is a gift from Dr. Fang Lin at the University of Iowa. The mcherry-CAAX construct is from lab stock (Lin et al., 2010). Plasmids are linearized and in vitro transcription is performed using the mMessage mMachine in vitro transcription kit (Ambion, Life Technologies) to make RNAs.

The amount of RNAs injected into the embryos are as follows: Centrin-GFP: 60pg; mcherry-CAAX: 50pg; GFP-Pk: 200pg.

Total RNA was extracted from uninjected and MO-injected embryos and converted to cDNA by in vitro reverse transcription. PCR used primers 5′-GTGAGATACTGCAACAGTCTG-3′ and 5′-ATACAAGGACTCGAAGCAGGT-3′ for *pk2* with Choice Taq DNA polymerase (Denville Scientific Inc.) in 35 cycles with the annealing temperature of 59 °C. Products were run on a 2% agarose gel, purified from the gel band and cloned into pCR™II Vector (Life Technologies) for sequencing.

Immunohistochemistry and cilia length measurements

Antibody staining was performed as described previously (Westfall et al., 2003). Embryos were fixed at 8 to 10 somite stages in 4% paraformaldehyde in 1xPBS. Anti-acetylated tubulin primary antibodies (Sigma) are used at a concentration of 1:800 and fluorescent secondary antibodies (Life Technologies) are used at a dilution of 1:400. Cilia length is measured in the Leica Lite software and the average cilia length of all measured embryos in each treatment group is calculated. ANOVA test is used to detect any statistical difference.

Whole mount in situ hybridization

Whole mount in situ hybridization was performed according to previously described protocols (Thisse et al., 1993; Westfall et al., 2003). Embryos were fixed at 76–78 hpf in 4% paraformaldehyde in 1xPBS. Digoxigenin-UTP labeled RNA riboprobes were made from linearized constructs using the MAXIscript in vitro transcription kit (Ambion, Life Technologies).

Retina preparation

Control and injected larvae are fixed at 76–78 hpf in 4% paraformaldehyde in 1xPBS overnight. Larvae are soaked first in 15% then 30% sucrose solution for at least 1h at room temperature and left in OCT at 4 °C overnight. Larvae are then aligned and embedded in OCT (Sakura), frozen and sectioned at a thickness of 12μm. Sections are left dry overnight, rehydrated in 1xPBS and stained by TOPRO3 (1:1000 in PBS). After PBS washes following TOPRO3 (Life Technologies), sections are mounted in VectaShield mounting medium (Vector Laboratories) and cover-slipped for imaging.

Light and confocal microscopy

KV morphology images were taken using a stereoscope with a Zeiss camera and Axiovision software. Confocal imaging was done on a Leica SP2 microscope system (Leica). For cilia imaging, embryos were dissected so the KV can be mounted on bridged cover slips with Vectashield (Vector Laboratories). Imaging was done with a 63x oil objective and a 2x digital zoom. Series of images were collected with 1μm interval. Maximum projection was used for quantification in the Leica software. For live neural tube imaging, embryos were treated with tricaine and mounted in 1% low melt agarose with their dorsal side against the coverslip. Imaging was done with a 63x oil objective and 2x digital zoom. Quantification was done on single scanned images by counting cell numbers.

Immunoprecipitation assay

Protein samples were prepared from mouse testes as described previously (Zhang et al., 2013) and the BBSome are precipitated with antibody against BBS2 as described previously (Zhang et al., 2013; Zhang et al., 2012).

Intracellular transport assays

5 dpf larvae were used for transport assays. Dark-reared embryos were treated with epinephrine (500 μg/ml, Sigma) and the time it takes for them to retract their melanosomes to the perinuclear region was recorded. The average time for all the larvae in each treatment group is calculated and statistical difference is detected by ANOVA test. Light-reared embryos were treated with caffeine (300 μg/ml, Sigma) and the number of larvae that show a response within 15 min, 35 min, or longer are counted. Chi-square test is used to detect any statistical difference between groups. Melanosome transport movies were taken using a stereoscope with a Zeiss camera and Axiovision software.

RESULTS

Zebrafish *pk2* modulates CE and retinal neurogenesis

In zebrafish, *pk1a* and other PCP components were shown to regulate convergence and extension during gastrulation (Bassuk et al., 2008; Lin et al., 2010; Roszko et al., 2009; Tada et al., 2003; Veeman et al., 2003). Our previous work has also shown that *pk1a* regulates retinal neurogenesis (Mei et al., 2013). Here we tested whether *pk2* knockdown disrupts CE and retinal patterning using an antisense morpholino oligonucleotide (MO). Efficiency of knockdown by a splice block MO was monitored by RT-PCR. The splice block MO generated an aberrant shorter *pk2* transcript through 5 day post fertilization (dpf). The aberrant transcript was the result of mis-splicing that removed the beginning of exon 5 resulting in a premature stop codon (Fig. S1 and data not shown). This MO generated a dose-dependent response for the phenotypes we evaluated in this paper (Supplemental Table 1). Similar to *pk1a* (Mei et al., 2013), *pk2* knockdown embryos displayed shorter antero-posterior axis and body curvature (Fig. 1A–D).

pk1a knockdown leads to a retinal neurogenesis defect in the inner plexiform layer (IPL) (Mei et al., 2013). The IPL harbors synaptic connections between ganglion cells and inner nuclear layer cells (Robles and Baier, 2012). We first determined the expression of *pk2* in the retina by whole-mount in situ hybridization and find that *pk2* is expressed in the retinal ganglion cell layer and inner nuclear layer (Fig. 1E–F). To visualize the IPL, we performed gene knockdown in a transgenic line HuC:GFP that expresses GFP in ganglion cells and a subset of amacrine cells (Link et al., 2000; Park et al., 2000). The processes from these neurons form two parallel sublaminae in the IPL (Lin et al., 2010; Link et al., 2000; Park et al., 2000). Previous work in our lab has shown that knockdown of *wnt5b*, the receptor *ryk* as well as *pk1a* all lead to disorganization of the sublaminae in the IPL (Lin et al., 2010). Here we found that *pk2* knockdown embryos also display disorganization of the sublaminae, as seen by a loss of continuous tracks in the IPL (Fig. 1). This defect in the IPL could be partially suppressed by *pk2* RNA (Fig. S2). Thus, similar to *pk1a*, *pk2* also plays a role in CE and in retinal neurogenesis.

Analysis of *pk2* and *bbs7* in shared phenotypes in the Kupffer's Vesicle

To dissect possible functional interactions between *pk2* and *bbs7*, we analyzed shared and individual phenotypes. The KV is a transient ciliated organ at the tailbud of the developing embryo during somite stages and it is important for left-right patterning. KV morphogenesis is altered by knockdown of *bbs* genes, characterized by smaller or absent KV, which we scored as abnormal (Fig. 2A–B) (Yen et al., 2006). We used a *bbs7* MO that generated dose-dependent response in the embryos (Supplemental Table 2) (Yen et al., 2006). Both *bbs7* knockdown (Supplemental Table 2) and *pk2* knockdown disrupted KV morphogenesis (Fig. 2A–B, supplemental table 3) suggesting that *pk2* and *bbs7* may function in a similar pathway. Synergistic interaction between BBS proteins was previously determined using combined knockdown and we found that *bbs7* was highly interactive with other BBS genes (Tayeh et al., 2008). To test for interaction between *bbs7* and *pk2*, we selected a dose of *pk2* MO that generates a low percentage of KV defects in the individual knockdown, between 10% and 15% (Fig. 2C). In addition, to ensure accurate comparisons between injected groups, the sequential injection strategy was used. In this approach, a clutch of embryos was injected with one MO and the group is split with a subset injected with the second MO (see methods). The percentage of KV defects in double knockdown was higher than either single MO independent of the order of MO delivery (Fig. 2C, S3). This trend held true for a different dose of *pk2* MO (Fig. S4). The KV morphology defects appeared to be additive and not the synergistic interaction that we have previously observed between BBS7 and other BBS genes.

pk2 and *bbs7* in KV cilia length control

KV morphogenesis requires proper migration of the precursor cells (Schneider et al., 2008), proper lumen formation (Oteiza et al., 2010) as well as ciliogenesis (Tayeh et al., 2008; Yen et al., 2006). A role for *pk1a* in KV lumen formation and ciliogenesis has been demonstrated (Oteiza et al., 2010) and *bbs* genes were shown to regulate KV cilia maintenance (Baye et al., 2011; Pretorius et al., 2010; Tayeh et al., 2008; Yen et al., 2006). To quantitate the interactions between *pk2* and *bbs7* in the KV cilia, we measured the cilia length by labeling cilia with an antibody against acetylated α-tubulin (Fig. 2D–E). At 8 to 10 somite stage, control embryos showed an average cilia length of 3.84±0.07 μm (n=8) (Fig. 2F). The length of cilia was shortened in *bbs7* MO injected embryos (3.25±0.08 μm, $p<0.01$, n=5) and in *pk2* MO injected embryos (2.67±0.08μm $p<0.01$, n=5) (Fig. 2F). Thus, individual knockdown of *bbs7* or *pk2* lead to shortened cilia. Using sequential injections we found that the cilia length in double knockdown embryos (2.74±0.07μm, $p<0.01$, n=6) was comparable to that of the single knockdown embryos, specifically, it was not significantly different from *pk2* knockdown (Fig. 2F). Of note, cilia length changes were independent of the KV morphology that was scored as either small or normal (data not shown). The observation that "normal sized" KVs still showed a cilia length defect suggested that KV morphogenesis scoring underestimates the penetrance of knockdown. In addition, the similar cilia length in double and single knockdown embryos is consistent with our observation that *pk2* and *bbs7* do not act in synergy.

Neural tube polarity defects in *pk2* and *bbs7* knockdown

KV morphology and cilia length data suggest that *bbs7* and *pk2* do not directly interact. We then directly tested *bbs7* functions in cell polarity by examining the polarity of the cells in the neural tube. Centrioles are placed medially in neural tube cells and this pattern has been used as a marker for cell polarity (Borovina et al., 2010). We asked if *pk2* or *bbs7* function was required for centriole placement by examining Centrin-GFP localization in live embryos. In control embryos, Centrin-GFP was localized toward the midline in the elongated dorsal neural tube cells (Fig. 3A). In the low-dose *pk2* MO- and *bbs7* MO-injected embryos, the cell shape was maintained, however, some cells had lateral placement of Centrin-GFP (Fig. 3B–D), suggesting mislocalization of basal bodies. We then tested Centrin localization in *pk2* and *bbs7* double knockdown embryos. We also found a milocalization of Centrin-GFP. To quantify the extent of defect, we measured the distance from Centrin to the midline (Fig. 3E). In control embryos, the distance was 2.48±0.22μm. In individual knockdown of *pk2* and of *bbs7*, the distance of Centrin from the midline was 3.82±0.40μm and 3.33±0.36μm, respectively. Although a greater distance from the midline than in control, the difference is not significant (Fig. 3E). However, double knockdown embryos displayed a statistically significant increase in the distance, at 4.88±0.48μm, compared to the control group ($p<0.01$) and to individual *bbs7* knockdown ($p<0.05$) (Fig. 3E). In addition, we observed disrupted Centrin localization without severe cell shape changes in the neural tube in knockdown embryos. Centrin-GFP localization in double knockdown was not significantly different from *pk2* single knockdown, indicating that the two genes affect similar process in parallel or independent pathways.

Asymmetric Pk localization in *bbs7* knockdown embryos

We demonstrated a Centrin localization defect in *bbs7* knockdown, a new phenotype that has not been described for BBS. We next set out to determine if the *bbs7*neural tube polarity-related defect is mediated through *pk*. PCP components such as Pk show asymmetric localization in polarized cells (Tree et al., 2002). In zebrafish, GFP-tagged *Drosophila* Pk (GFP-Pk) shows asymmetric localization in puncta adjacent to the anterior cell membrane in the neural tube (Yin et al., 2008). This localization is disrupted in PCP related mutants (Hayes et al., 2013; Yin et al., 2008). We tested whether *bbs7* knockdown alters Pk localization. GFP-Pk with a membrane marker mcherry-CAAX was mosaically expressed in control and *bbs7* knockdown embryos (Fig. 4A–B). In the control embryos, approximately 50% of GFP-positive cells showed Pk puncta adjacent to the anterior membrane (Fig. 4C). In *bbs7* knockdown embryos, we observe asymmetric localization of GFP-Pk puncta, to the same extent as that of the control embryos (Fig. 4C). These data suggest that while *bbs7* knockdown leads to Centrin mislocalization, *bbs7* activity is not required for the asymmetric localization of Pk in the neural tube.

BBSome formation in *Pk2* mutant mouse

Bbs7 is a core component of the BBSome that also interacts with the chaperonin complex (Zhang et al., 2012). Manipulation of any BBSome component leads to disruption of the complex (Zhang et al., 2013; Zhang et al., 2012). Thus, we evaluated BBSome assembly in the absence of *pk2*. Due to the lack of Bbs antibodies for biochemical analysis in the

zebrafish model, we utilized the mutant mice for *Pk2*. A viable *Pk2* mutant ($Pk2^{-/-}$) is available that has a neomycin insertion encompassing exon 4–6 and it is thought to be a null allele (Tao et al., 2011). BBSome components were isolated by immunoprecipitation from mouse testis samples. We found BBSome assembly in $Pk2^{-/-}$ mutant was similar to wild-type littermates (Fig. 4D). These data suggest that *Pk2* is not required for BBSome assembly. Together with KV morphology and cilia length data, our localization and protein interaction results support the hypothesis that *pk2* and *bbs7* act independently in different pathways that in specific tissue contexts converge on the same processes.

pk2 knockdown suppresses the *bbs7*-related intracellular transport defect

We have shown that *bbs7* plays a role in neural tube cell polarity but it does not affect Pk asymmetrical localization. To further probe the relationship between bbs7 and pk2, we addressed the question whether *pk2* modulates any other *bbs7*-related functions. One of the cardinal features of *bbs* knockdown is a delay of the retrograde trafficking of melanosomes in melanocytes (Yen et al., 2006). Thus, we investigated melanosome transport in individual and double knockdown of *pk2* and *bbs7*. Pigment redistribution is an adaptive response in zebrafish. In response to light, melanosomes relocate from a dispersed state to a perinuclear location in melanocytes (Fig. 5A). The trafficking of melanosomes can be chemically stimulated and the rate of transport can be monitored. In dark-reared larvae, application of epinephrine promotes retrograde melanosome transport, from dispersed to perinuclear distribution (Supplemental movie S1). Under standard conditions, 5 days post fertilization (dpf) wild-type larvae retract melanosomes within ~100 seconds (Fig. 5C). As previously reported (Yen et al., 2006), *bbs7* knockdown leads to a statistically significant delay (Fig. 5C). Individual knockdown of *pk2* did not show a transport delay. Surprisingly in the combined *bbs7* and *pk2* knockdown, we saw a suppression of the *bbs7*-induced delay (Fig. 5C). Statistically significant suppression was observed independent of the order of the sequential injection (Fig. S4).

The *pk2* mediated suppression of the *bbs7*-related transport delay lends insight into the nature of the interaction. Phenotypic suppression was reported for intraflagellar transport complex (IFT) components (Ocbina et al., 2011). Loss of an anterograde IFT gene *Ift172* suppresses the cilia defects in homozygous mutants *Dync2h1*, a retrograde ciliary motor (Ocbina et al., 2011). To determine if *pk2* was acting by a similar mechanism, we tested anterograde transport. In light-reared zebrafish, caffeine can be used to promote anterograde transport of melanosomes from perinuclear to disperse. The rate of transport was slower than retrograde, therefore the data were grouped by the number of embryos that responded within a given segment of time (0–15min, 16–35 min and longer than 35 min). Almost half of wild-type larvae responded within 15 min and the rest by 35 min (Fig. 6A). As previously reported, *bbs7* knockdown did not alter the rate of anterograde transport (Yen et al., 2006) and we saw a similar distribution in *bbs7* MO injected larvae compared to uninjected larvae (Fig. 6A). As a control, we used gene knockdown of *ift22*, an IFT component important for anterograde movement (Lucker et al., 2010; Sung and Leroux, 2013), and we found a significant delay in anterograde transport. In addition, *pk2* knockdown also led to a statistically significant delay (Fig. 6A). We then posit that *ift22* knockdown would suppress *bbs7*-knockdown induced retrograde transport delay. Individual knockdown of *ift22* did not

lead to a retrograde transport delay (Fig. 6B). Yet, there was suppression of the *bbs7*-related delay (Fig. 6B). This result combined with *pk2* related delay in anterograde transport suggests a novel role for *pk2* in intracellular transport, and further support that *bbs7* and *pk2* modulate distinct pathways.

DISCUSSION

BBS is a cilia-related disorder and BBS functional mechanisms are known to require formation of two complexes and trafficking of cellular components. PCP components have been implicated in cilia orientation and PCP components such as Dvl localize to the basal bodies. While BBS has been implicated in PCP, there are conflicting reports. Here we investigate the relatedness of BBS to cell polarity using *Pk2*, a core PCP component, and *Bbs7,* which interacts with both BBS-related complexes. Using knockdown of *bbs7* and *pk2* genes, we test for interactions in different tissue contexts in the zebrafish and also investigate BBS complex formation in mouse *Pk2* knockouts. Analyzing KV morphology, cilia length and neural tube polarity, we find an apparent additive effect without synergy in double knockdown of *bbs7* and *pk2*. In marked contrast, *pk2* knockdown suppresses the *bbs7*-related melanosome retrograde transport defect, suggesting a novel role for *pk2* in intracellular transport.

Our analyses with KV morphology and cilia length support overlapping but distinct functions of *pk2* and *bbs7*. While the double knockdown KV morphology phenotype appears to be additive, we find similar cilia length in double knockdown and single knockdown embryos. These data suggest that KV morphogenesis can be uncoupled from KV ciliogenesis. This is consistent with published reports in which reduced KV lumen can have normal cilia length (Tay et al., 2013). Moreover, KV formation is a multistep process requiring proper migration and adhesion of precursor cells, lumenogenesis and ciliogenesis (Oteiza et al., 2010; Schneider et al., 2008; Tayeh et al., 2008; Yen et al., 2006). Pk1a in zebrafish is involved in organization of the KV precursors, adhesion and cilia length (Oteiza et al., 2010). Thus, KV morphology takes into account *pk2* function that might be unrelated to ciliogenesis. In addition, we observed normal KV morphology with shortened cilia. We reason that these cilia are still sufficient to generate fluid flow for proper KV morphogenesis. It is worth to note that, in our cilia length analyses, we did not observe changes in the number of cilia per embryo. Thus, combining the KV morphology and cilia length analyses, we conclude that *bbs7* and *pk2* show overlapping functions in the KV, but no direct genetic interactions, suggesting they act in distinct pathways.

Polarity in the neural tube has been proposed as a readout for vertebrate PCP (Borovina et al., 2010). While PCP mutants have been shown to disrupt neural tube polarity (Hayes et al., 2013; Yin et al., 2008) it has not been demonstrated for BBS. We find that *pk2* knockdown leads to altered Centrin localization in the neural tube, and *bbs7* knockdown also disrupts Centrin localization. Yet, this *bbs7*-related neural tube defect appears to be independent of PCP as *bbs7* morphants do not show altered asymmetric Pk-GFP localization. Taken together, these data indicate that the polarization of the neural tube requires overlapping networks and that *bbs7* and *pk2* may be acting in distinct pathways. Consistently, *pk2* is not required for BBSome assembly. The BBSome complex forms in $Pk2^{-/-}$ mutant mouse

testis. While we cannot rule out the contributions of other murine *Prickle* genes in other tissues, the combined zebrafish and mouse data lead us to conclude that *Bbs7* and *Pk2* are in distinct pathways that when mutated result in overlapping phenotypes.

In this study, we find a novel role for *pk2* in anterograde intracellular transport. Whether *pk2* has a similar function in ciliary transport remains to be determined. The core PCP protein Dvl is shown to localize to the basal body and regulate its membrane docking (Hashimoto et al., 2010; Mahuzier et al., 2012; Park et al., 2008; Zilber et al., 2013). Additionally, a PCP effector, Fuzzy, has a role in protein trafficking at the base of the cilia (Heydeck et al., 2009; Zilber et al., 2013). Therefore PCP may generally play a role at the basal body by affecting its docking and protein loading to achieve proper cilia orientation. In the mouse node, the basal body and cilium is posteriorly oriented while Pk2 localizes to the anterior/posterior membrane boundary (Antic et al., 2010; Hashimoto et al., 2010). Therefore, *pk2* may act in intracellular transport in general rather than transport at the highly specified basal body and cilium. Future studies visualizing Pk2 localization and particle trafficking will determine the extent to which Pk2 is directly involved in anterograde transport, similar to some IFT proteins.

BBS is a cilia-related disorder and BBS proteins function to regulate trafficking in the cilia, as well as playing a role in intracellular trafficking such as melanosome trafficking in zebrafish. We report that *pk2* knockdown suppresses the *bbs7*-related retrograde transport defect. Interestingly, we did not observe a similar suppression of KV cilia length defects. The double knockdown embryos still display shortened cilia comparable to single knockdown embryos. Ciliogenesis is a process in which the centrosome matures into the basal body which then docks at the cell membrane before axoneme extension (Sung and Leroux, 2013). In fact, cilia length is controlled by factors including timing of the cell cycle, intraflagellar transport, and additional molecular pathways (Avasthi and Marshall, 2012; Ishikawa and Marshall, 2011). *bbs7* most likely affects KV ciliogenesis via its role in intraflagellar transport while *pk2* also influences other aspects including polarized cell movement of the KV precursors, KV lumen formation and cilia tilt (Borovina et al., 2010; Oteiza et al., 2010). Thus the additional tissue-specific functions of Pk2 in KV formation and then ciliogenesis of the KV may not be countered by BBS gene knockdown. The need for polarized cell migration, adhesion and lumen formation is not required in melanocytes and analysis in this tissue allows us to uncover a novel interaction between BBS and prickle pathways. Our study provides a useful system that can be used to dissect gene-gene interactions.

In summary, we have functionally characterized the role of *bbs7* and *pk2* in the ciliated KV, neural tube and melanocytes. Our interaction study suggests an indirect interaction between *bbs7* and *pk2*. They act in distinct pathways that converge on different processes. In the melanocytes, we uncover a novel role for *pk2* in intracellular transport. Our work here clarifies the link between PCP and BBS and future work will focus on the detailed role of *pk2* in intracellular transport.

Supplementary Material

Refer to Web version on PubMed Central for supplementary material.

Acknowledgments

We thank Dr. Douglas W. Houston and Dr. Daniel F. Eberl for their comments on the manuscript.

FUNDING This work is supported by the National Institute of Health [1R01NS064159-01A1 to A.G.B and D.C.S; 1R21MH100086-01 to A.G.B; 5R01EY017168 to V.C.S. AND D.C.S.; AND 5R01EY011298 to V.C.S.].

References

Aldahmesh MA, Li Y, Alhashem A, Anazi S, Alkuraya H, Hashem M, Awaji AA, Sogaty S, Alkharashi A, Alzahrani S, Al Hazzaa SA, Xiong Y, Kong S, Sun Z, Alkuraya FS. IFT27, encoding a small GTPase component of IFT particles, is mutated in a consanguineous family with Bardet-Biedl syndrome. Human molecular genetics. 2014

Antic D, Stubbs JL, Suyama K, Kintner C, Scott MP, Axelrod JD. Planar cell polarity enables posterior localization of nodal cilia and left-right axis determination during mouse and Xenopus embryogenesis. PloS one. 2010; 5:e8999. [PubMed: 20126399]

Avasthi P, Marshall WF. Stages of ciliogenesis and regulation of ciliary length. Differentiation; research in biological diversity. 2012; 83:S30–42.

Balciuniene J, Nagelberg D, Walsh KT, Camerota D, Georlette D, Biemar F, Bellipanni G, Balciunas D. Efficient disruption of Zebrafish genes using a Gal4-containing gene trap. BMC genomics. 2013; 14:619. [PubMed: 24034702]

Bardet G. On congenital obesity syndrome with polydactyly and retinitis pigmentosa (a contribution to the study of clinical forms of hypophyseal obesity). 1920. Obesity research. 1995; 3:387–399. [PubMed: 8521156]

Bassuk AG, Wallace RH, Buhr A, Buller AR, Afawi Z, Shimojo M, Miyata S, Chen S, Gonzalez-Alegre P, Griesbach HL, Wu S, Nashelsky M, Vladar EK, Antic D, Ferguson PJ, Cirak S, Voit T, Scott MP, Axelrod JD, Gurnett C, Daoud AS, Kivity S, Neufeld MY, Mazarib A, Straussberg R, Walid S, Korczyn AD, Slusarski DC, Berkovic SF, El-Shanti HI. A homozygous mutation in human PRICKLE1 causes an autosomal-recessive progressive myoclonus epilepsy-ataxia syndrome. American journal of human genetics. 2008; 83:572–581. [PubMed: 18976727]

Baye LM, Patrinostro X, Swaminathan S, Beck JS, Zhang Y, Stone EM, Sheffield VC, Slusarski DC. The N-terminal region of centrosomal protein 290 (CEP290) restores vision in a zebrafish model of human blindness. Human molecular genetics. 2011; 20:1467–1477. [PubMed: 21257638]

Biedl A. A pair of siblings with adiposo-genital dystrophy. 1922. Obesity research. 1995; 3:404. [PubMed: 8521158]

Blacque OE, Leroux MR. Bardet-Biedl syndrome: an emerging pathomechanism of intracellular transport. Cellular and molecular life sciences : CMLS. 2006; 63:2145–2161. [PubMed: 16909204]

Borovina A, Ciruna B. IFT88 Plays a Cilia- and PCP-Independent Role in Controlling Oriented Cell Divisions during Vertebrate Embryonic Development. Cell reports. 2013; 5:37–43. [PubMed: 24095732]

Borovina A, Superina S, Voskas D, Ciruna B. Vangl2 directs the posterior tilting and asymmetric localization of motile primary cilia. Nature cell biology. 2010; 12:407–412.

Fan Y, Esmail MA, Ansley SJ, Blacque OE, Boroevich K, Ross AJ, Moore SJ, Badano JL, May-Simera H, Compton DS, Green JS, Lewis RA, van Haelst MM, Parfrey PS, Baillie DL, Beales PL, Katsanis N, Davidson WS, Leroux MR. Mutations in a member of the Ras superfamily of small GTP-binding proteins causes Bardet-Biedl syndrome. Nature genetics. 2004; 36:989–993. [PubMed: 15314642]

Gerdes JM, Liu Y, Zaghloul NA, Leitch CC, Lawson SS, Kato M, Beachy PA, Beales PL, DeMartino GN, Fisher S, Badano JL, Katsanis N. Disruption of the basal body compromises proteasomal

function and perturbs intracellular Wnt response. Nature genetics. 2007; 39:1350–1360. [PubMed: 17906624]

Green JS, Parfrey PS, Harnett JD, Farid NR, Cramer BC, Johnson G, Heath O, McManamon PJ, O'Leary E, Pryse-Phillips W. The cardinal manifestations of Bardet-Biedl syndrome, a form of Laurence-Moon-Biedl syndrome. The New England journal of medicine. 1989; 321:1002–1009. [PubMed: 2779627]

Hashimoto M, Shinohara K, Wang J, Ikeuchi S, Yoshiba S, Meno C, Nonaka S, Takada S, Hatta K, Wynshaw-Boris A, Hamada H. Planar polarization of node cells determines the rotational axis of node cilia. Nature cell biology. 2010; 12:170–176.

Hayes M, Naito M, Daulat A, Angers S, Ciruna B. Ptk7 promotes non-canonical Wnt/PCP-mediated morphogenesis and inhibits Wnt/beta-catenin-dependent cell fate decisions during vertebrate development. Development. 2013; 140:1807–1818. [PubMed: 23533179]

Heydeck W, Zeng H, Liu A. Planar cell polarity effector gene Fuzzy regulates cilia formation and Hedgehog signal transduction in mouse. Developmental dynamics : an official publication of the American Association of Anatomists. 2009; 238:3035–3042. [PubMed: 19877275]

Huang P, Schier AF. Dampened Hedgehog signaling but normal Wnt signaling in zebrafish without cilia. Development. 2009; 136:3089–3098. [PubMed: 19700616]

Ishikawa H, Marshall WF. Ciliogenesis: building the cell's antenna. Nature reviews Molecular cell biology. 2011; 12:222–234.

Jenny A, Darken RS, Wilson PA, Mlodzik M. Prickle and Strabismus form a functional complex to generate a correct axis during planar cell polarity signaling. The EMBO journal. 2003; 22:4409–4420. [PubMed: 12941693]

Jenny A, Reynolds-Kenneally J, Das G, Burnett M, Mlodzik M. Diego and Prickle regulate Frizzled planar cell polarity signalling by competing for Dishevelled binding. Nature cell biology. 2005; 7:691–697.

Jiang D, Munro EM, Smith WC. Ascidian prickle regulates both mediolateral and anterior-posterior cell polarity of notochord cells. Curr Biol. 2005; 15:79–85. [PubMed: 15700379]

Jin H, White SR, Shida T, Schulz S, Aguiar M, Gygi SP, Bazan JF, Nachury MV. The conserved Bardet-Biedl syndrome proteins assemble a coat that traffics membrane proteins to cilia. Cell. 2010; 141:1208–1219. [PubMed: 20603001]

Jones C, Roper VC, Foucher I, Qian D, Banizs B, Petit C, Yoder BK, Chen P. Ciliary proteins link basal body polarization to planar cell polarity regulation. Nature genetics. 2008; 40:69–77. [PubMed: 18066062]

Kimmel CB, Ballard WW, Kimmel SR, Ullmann B, Schilling TF. Stages of embryonic development of the zebrafish. Developmental dynamics : an official publication of the American Association of Anatomists. 1995; 203:253–310. [PubMed: 8589427]

Lin S, Baye LM, Westfall TA, Slusarski DC. Wnt5b-Ryk pathway provides directional signals to regulate gastrulation movement. The Journal of cell biology. 2010; 190:263–278. [PubMed: 20660632]

Link BA, Fadool JM, Malicki J, Dowling JE. The zebrafish young mutation acts non-cell-autonomously to uncouple differentiation from specification for all retinal cells. Development. 2000; 127:2177–2188. [PubMed: 10769241]

Loktev AV, Zhang Q, Beck JS, Searby CC, Scheetz TE, Bazan JF, Slusarski DC, Sheffield VC, Jackson PK, Nachury MV. A BBSome subunit links ciliogenesis, microtubule stability, and acetylation. Developmental cell. 2008; 15:854–865. [PubMed: 19081074]

Lucker BF, Miller MS, Dziedzic SA, Blackmarr PT, Cole DG. Direct interactions of intraflagellar transport complex B proteins IFT88, IFT52, and IFT46. The Journal of biological chemistry. 2010; 285:21508–21518. [PubMed: 20435895]

Mahuzier A, Gaude HM, Grampa V, Anselme I, Silbermann F, Leroux-Berger M, Delacour D, Ezan J, Montcouquiol M, Saunier S, Schneider-Maunoury S, Vesque C. Dishevelled stabilization by the ciliopathy protein Rpgrip1l is essential for planar cell polarity. The Journal of cell biology. 2012; 198:927–940. [PubMed: 22927466]

Mapp OM, Walsh GS, Moens CB, Tada M, Prince VE. Zebrafish Prickle1b mediates facial branchiomotor neuron migration via a farnesylation-dependent nuclear activity. Development. 2011; 138:2121–2132. [PubMed: 21521740]

Mapp OM, Wanner SJ, Rohrschneider MR, Prince VE. Prickle1b mediates interpretation of migratory cues during zebrafish facial branchiomotor neuron migration. Developmental dynamics : an official publication of the American Association of Anatomists. 2010; 239:1596–1608. [PubMed: 20503357]

Marshall WF, Nonaka S. Cilia: tuning in to the cell's antenna. Curr Biol. 2006; 16:R604–614. [PubMed: 16890522]

May-Simera HL, Kai M, Hernandez V, Osborn DP, Tada M, Beales PL. Bbs8, together with the planar cell polarity protein Vangl2, is required to establish left-right asymmetry in zebrafish. Developmental biology. 2010; 345:215–225. [PubMed: 20643117]

Mei X, Wu S, Bassuk AG, Slusarski DC. Mechanisms of prickle1a function in zebrafish epilepsy and retinal neurogenesis. Disease models & mechanisms. 2013; 6:679–688. [PubMed: 23324328]

Montcouquiol M, Rachel RA, Lanford PJ, Copeland NG, Jenkins NA, Kelley MW. Identification of Vangl2 and Scrb1 as planar polarity genes in mammals. Nature. 2003; 423:173–177. [PubMed: 12724779]

Nachury MV, Loktev AV, Zhang Q, Westlake CJ, Peranen J, Merdes A, Slusarski DC, Scheller RH, Bazan JF, Sheffield VC, Jackson PK. A core complex of BBS proteins cooperates with the GTPase Rab8 to promote ciliary membrane biogenesis. Cell. 2007; 129:1201–1213. [PubMed: 17574030]

Ng J. Wnt/PCP proteins regulate stereotyped axon branch extension in Drosophila. Development. 2012; 139:165–177. [PubMed: 22147954]

Ocbina PJ, Eggenschwiler JT, Moskowitz I, Anderson KV. Complex interactions between genes controlling trafficking in primary cilia. Nature genetics. 2011; 43:547–553. [PubMed: 21552265]

Oteiza P, Koppen M, Krieg M, Pulgar E, Farias C, Melo C, Preibisch S, Muller D, Tada M, Hartel S, Heisenberg CP, Concha ML. Planar cell polarity signalling regulates cell adhesion properties in progenitors of the zebrafish laterality organ. Development (Cambridge, England). 2010; 137:3459–3468.

Park HC, Kim CH, Bae YK, Yeo SY, Kim SH, Hong SK, Shin J, Yoo KW, Hibi M, Hirano T, Miki N, Chitnis AB, Huh TL. Analysis of upstream elements in the HuC promoter leads to the establishment of transgenic zebrafish with fluorescent neurons. Developmental biology. 2000; 227:279–293. [PubMed: 11071755]

Park TJ, Mitchell BJ, Abitua PB, Kintner C, Wallingford JB. Dishevelled controls apical docking and planar polarization of basal bodies in ciliated epithelial cells. Nature genetics. 2008; 40:871–879. [PubMed: 18552847]

Pasqualato S, Renault L, Cherfils J. Arf, Arl, Arp and Sar proteins: a family of GTP-binding proteins with a structural device for 'front-back' communication. EMBO reports. 2002; 3:1035–1041. [PubMed: 12429613]

Pretorius PR, Baye LM, Nishimura DY, Searby CC, Bugge K, Yang B, Mullins RF, Stone EM, Sheffield VC, Slusarski DC. Identification and functional analysis of the vision-specific BBS3 (ARL6) long isoform. PLoS genetics. 2010; 6:e1000884. [PubMed: 20333246]

Qian D, Jones C, Rzadzinska A, Mark S, Zhang X, Steel KP, Dai X, Chen P. Wnt5a functions in planar cell polarity regulation in mice. Developmental biology. 2007; 306:121–133. [PubMed: 17433286]

Robles E, Baier H. Assembly of synaptic laminae by axon guidance molecules. Current opinion in neurobiology. 2012; 22:799–804. [PubMed: 22632825]

Ross AJ, May-Simera H, Eichers ER, Kai M, Hill J, Jagger DJ, Leitch CC, Chapple JP, Munro PM, Fisher S, Tan PL, Phillips HM, Leroux MR, Henderson DJ, Murdoch JN, Copp AJ, Eliot MM, Lupski JR, Kemp DT, Dollfus H, Tada M, Katsanis N, Forge A, Beales PL. Disruption of Bardet-Biedl syndrome ciliary proteins perturbs planar cell polarity in vertebrates. Nature genetics. 2005; 37:1135–1140. [PubMed: 16170314]

Roszko I, Sawada A, Solnica-Krezel L. Regulation of convergence and extension movements during vertebrate gastrulation by the Wnt/PCP pathway. Seminars in cell & developmental biology. 2009; 20:986–997. [PubMed: 19761865]

Scheidecker S, Etard C, Pierce NW, Geoffroy V, Schaefer E, Muller J, Chennen K, Flori E, Pelletier V, Poch O, Marion V, Stoetzel C, Strahle U, Nachury MV, Dollfus H. Exome sequencing of Bardet-Biedl syndrome patient identifies a null mutation in the BBSome subunit BBIP1 (BBS18). Journal of medical genetics. 2014; 51:132–136. [PubMed: 24026985]

Schneider I, Houston DW, Rebagliati MR, Slusarski DC. Calcium fluxes in dorsal forerunner cells antagonize beta-catenin and alter left-right patterning. Development. 2008; 135:75–84. [PubMed: 18045845]

Seo S, Baye LM, Schulz NP, Beck JS, Zhang Q, Slusarski DC, Sheffield VC. BBS6, BBS10, and BBS12 form a complex with CCT/TRiC family chaperonins and mediate BBSome assembly. Proceedings of the National Academy of Sciences of the United States of America. 2010; 107:1488–1493. [PubMed: 20080638]

Singla V, Reiter JF. The primary cilium as the cell's antenna: signaling at a sensory organelle. Science. 2006; 313:629–633. [PubMed: 16888132]

Sung CH, Leroux MR. The roles of evolutionarily conserved functional modules in cilia-related trafficking. Nature cell biology. 2013; 15:1387–1397.

Tada M, Wilson S, Ueno N, Takeuchi M, Concha M, Carreira-Barbosa F. Prickle 1 regulates cell movements during gastrulation and neuronal migration in zebrafish. Development. 2003; 130:4037. [PubMed: 12874125]

Takeuchi M, Nakabayashi J, Sakaguchi T, Yamamoto TS, Takahashi H, Takeda H, Ueno N. The prickle-related gene in vertebrates is essential for gastrulation cell movements. Curr Biol. 2003; 13:674–679. [PubMed: 12699625]

Tao H, Inoue K, Kiyonari H, Bassuk AG, Axelrod JD, Sasaki H, Aizawa S, Ueno N. Nuclear localization of Prickle2 is required to establish cell polarity during early mouse embryogenesis. Developmental biology. 2012; 364:138–148. [PubMed: 22333836]

Tao H, Manak JR, Sowers L, Mei X, Kiyonari H, Abe T, Dahdaleh NS, Yang T, Wu S, Chen S, Fox MH, Gurnett C, Montine T, Bird T, Shaffer LG, Rosenfeld JA, McConnell J, Madan-Khetarpal S, Berry-Kravis E, Griesbach H, Saneto RP, Scott MP, Antic D, Reed J, Boland R, Ehaideb SN, El-Shanti H, Mahajan VB, Ferguson PJ, Axelrod JD, Lehesjoki AE, Fritzsch B, Slusarski DC, Wemmie J, Ueno N, Bassuk AG. Mutations in Prickle Orthologs Cause Seizures in Flies, Mice, and Humans. The American Journal of Human Genetics. 2011; 88:138–149.

Tao H, Suzuki M, Kiyonari H, Abe T, Sasaoka T, Ueno N. Mouse prickle1, the homolog of a PCP gene, is essential for epiblast apical-basal polarity. Proceedings of the National Academy of Sciences. 2009; 106:14426–14431.

Tay HG, Schulze SK, Compagnon J, Foley FC, Heisenberg CP, Yost HJ, Abdelilah-Seyfried S, Amack JD. Lethal giant larvae 2 regulates development of the ciliated organ Kupffer's vesicle. Development. 2013; 140:1550–1559. [PubMed: 23482490]

Tayeh MK, Yen HJ, Beck JS, Searby CC, Westfall TA, Griesbach H, Sheffield VC, Slusarski DC. Genetic interaction between Bardet-Biedl syndrome genes and implications for limb patterning. Human molecular genetics. 2008; 17:1956–1967. [PubMed: 18381349]

Thisse C, Thisse B, Schilling TF, Postlethwait JH. Structure of the zebrafish snail1 gene and its expression in wild-type, spadetail and no tail mutant embryos. Development. 1993; 119:1203–1215. [PubMed: 8306883]

Tree DRP, Shulman JM, Rousset R, Scott MP, Gubb D, Axelrod JD. Prickle Mediates Feedback Amplification to Generate Asymmetric Planar Cell Polarity Signaling. Cell. 2002; 109:371–381. [PubMed: 12015986]

Veeman MT, Slusarski DC, Kaykas A, Louie SH, Moon RT. Zebrafish prickle, a modulator of noncanonical Wnt/Fz signaling, regulates gastrulation movements. Current biology : CB. 2003; 13:680–685. [PubMed: 12699626]

Wang J, Mark S, Zhang X, Qian D, Yoo SJ, Radde-Gallwitz K, Zhang Y, Lin X, Collazo A, Wynshaw-Boris A, Chen P. Regulation of polarized extension and planar cell polarity in the cochlea by the vertebrate PCP pathway. Nature genetics. 2005; 37:980–985. [PubMed: 16116426]

Wang Y, Guo N, Nathans J. The role of Frizzled3 and Frizzled6 in neural tube closure and in the planar polarity of inner-ear sensory hair cells. The Journal of neuroscience : the official journal of the Society for Neuroscience. 2006; 26:2147–2156. [PubMed: 16495441]

Westerfield, M. The zebrafish book : a guide for the laboratory use of zebrafish (Brachydanio rerio). M. Westerfield; Eugene, OR: 1993.

Westfall TA, Hjertos B, Slusarski DC. Requirement for intracellular calcium modulation in zebrafish dorsal-ventral patterning. Developmental biology. 2003; 259:380–391. [PubMed: 12871708]

Yen HJ, Tayeh MK, Mullins RF, Stone EM, Sheffield VC, Slusarski DC. Bardet-Biedl syndrome genes are important in retrograde intracellular trafficking and Kupffer's vesicle cilia function. Human molecular genetics. 2006; 15:667–677. [PubMed: 16399798]

Yin C, Kiskowski M, Pouille PA, Farge E, Solnica-Krezel L. Cooperation of polarized cell intercalations drives convergence and extension of presomitic mesoderm during zebrafish gastrulation. The Journal of cell biology. 2008; 180:221–232. [PubMed: 18195109]

Zhang Q, Nishimura D, Seo S, Vogel T, Morgan DA, Searby C, Bugge K, Stone EM, Rahmouni K, Sheffield VC. Bardet-Biedl syndrome 3 (Bbs3) knockout mouse model reveals common BBS-associated phenotypes and Bbs3 unique phenotypes. Proceedings of the National Academy of Sciences of the United States of America. 2011; 108:20678–20683. [PubMed: 22139371]

Zhang Q, Nishimura D, Vogel T, Shao J, Swiderski R, Yin T, Searby C, Carter CS, Kim G, Bugge K, Stone EM, Sheffield VC. BBS7 is required for BBSome formation and its absence in mice results in Bardet-Biedl syndrome phenotypes and selective abnormalities in membrane protein trafficking. Journal of cell science. 2013; 126:2372–2380. [PubMed: 23572516]

Zhang Q, Yu D, Seo S, Stone EM, Sheffield VC. Intrinsic protein-protein interaction-mediated and chaperonin-assisted sequential assembly of stable bardet-biedl syndrome protein complex, the BBSome. The Journal of biological chemistry. 2012; 287:20625–20635. [PubMed: 22500027]

Zhang Y, Seo S, Bhattarai S, Bugge K, Searby CC, Zhang Q, Drack AV, Stone EM, Sheffield VC. BBS mutations modify phenotypic expression of CEP290-related ciliopathies. Human molecular genetics. 2014; 23:40–51. [PubMed: 23943788]

Zilber Y, Babayeva S, Seo JH, Liu JJ, Mootin S, Torban E. The PCP effector Fuzzy controls cilial assembly and signaling by recruiting Rab8 and Dishevelled to the primary cilium. Molecular biology of the cell. 2013; 24:555–565. [PubMed: 23303251]

Highlights

- *bbs7* and *pk2* both affect zebrafish neural tube polarity
- Bbs7 is not required for asymmetric Pk localization
- BBSome assembly is unperturbed in *Pk2* knockout mice.
- *pk2* knockdown suppresses *bbs7*-related retrograde melanosome transport defect.
- Pk2 modulates anterograde intracellular transport.

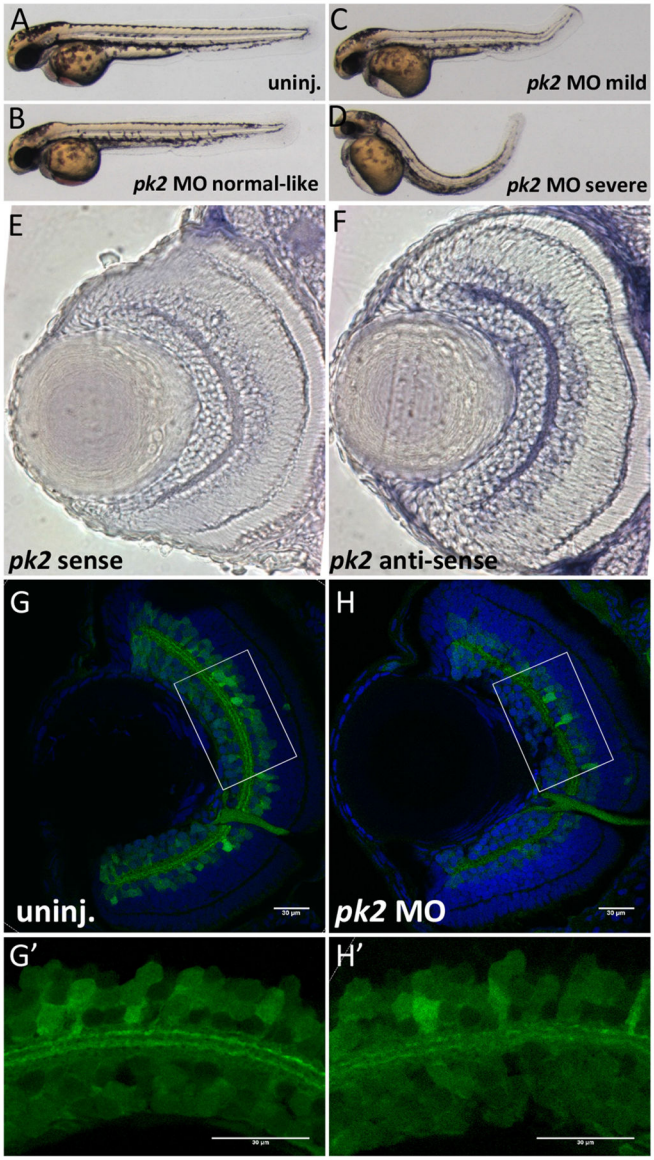

Figure 1. *pk2* knockdown leads to body curvature and IPL neurogenesis defects in zebrafish

A–D. Morphology of uninjected or *pk2* MO injected embryos at 28hpf. Injection of *pk2* MO leads to body curvature phenotypes at different severity, from normal like to severe. E–F. *pk2* expression in the retina sections. E, sense control; F, anti-sense. *pk2* is enriched in the ganglion cell layer and inner nuclear layer. G–H′. Retinal neurogenesis defects in *pk2* knockdown embryos. G–H, whole eye sections; G′–H′, zoom-in view of boxed areas in G–H. *pk2* knockdown leads to disorganization of inner plexiform layer synaptic connections, characterized by discontinuous layers. Scale bars are 30μm in each image.

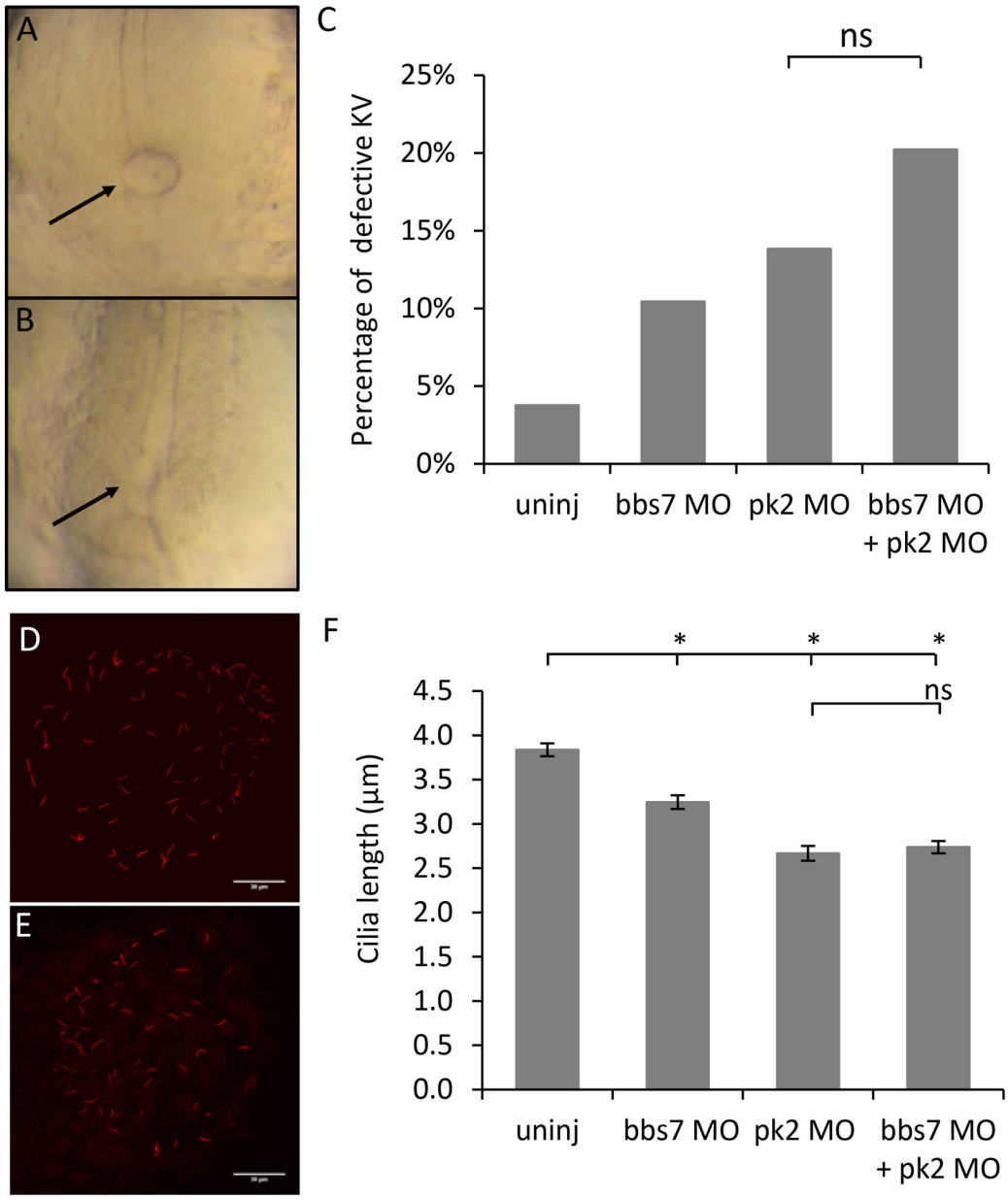

Figure 2. *pk2* and *bbs7* double knockdown shows no synergy in KV morphogenesis and KV cilia length

A–B. An example of a normal KV (A) and a reduced KV (B). C. Graph of percentage of KV defects. The double knockdown group show a KV defect that is comparable to each single knockdown group. *pk2* MO dose is 1.25ng. Uninj, n=159; *bbs7* MO, n=134; *pk2* MO, n=159; *bbs7* MO+*pk2* MO, n=173. ns, not significant by Fisher's Exact Test. D–E. An example of normal cilia (D) and reduced cilia (E) at 8–10SS. Scale bars are 30μm in each image. F. Graph of cilia length measurements. *bbs7* and *pk2* knockdown each leads to shortened cilia, and the double knockdown shows a defect that is comparable to each single knockdown group. Uninj, n=223; *bbs7* MO, n=201; *pk2* MO, n=141; *bbs7* MO+*pk2* MO,

n=191. Error bars are presented as standard error. *, p<0.01; ns, not significant; ANOVA with Tukey.

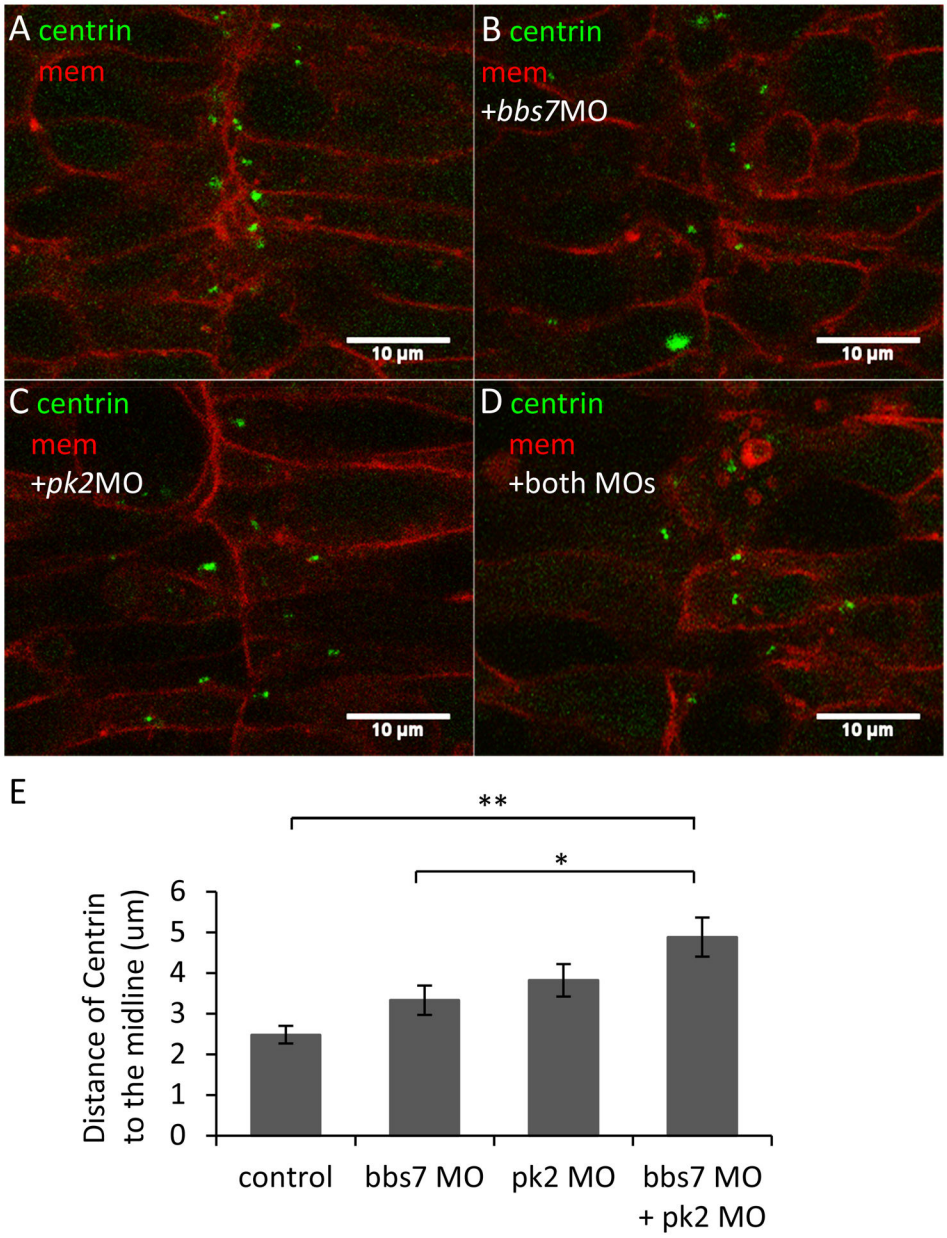

Figure 3. *pk2* and *bbs7* double knockdown shows defects in centriole placement in the neural tube

A–D. Centrin localization in the developing neural tube in *pk2* and *bbs7* single or double knockdown embryos. Green, Centrin-GFP; Red, mcherry-CAAX. In the control (A), centrin-GFP are localized close to the midline. In the single and double knockdown embryos (B–D), some cells have lateral placement of Centrin. Overall, the cell shape does not change. Scale bars are 10μm in each image. E. Quantification of distances of Centrin to the midline. While *bbs7* and *pk2* knockdown each leads to slight increase in the distance of Centrin to the midline, the double knockdown displays a significant increase in the distance. For control, n=119; *bbs7* MO, n=33, *pk2* MO, n=30, *bbs7* MO+*pk2* MO, n=45. Error bars are presented as standard error. **, $p<0.01$; *, $p<0.05$; ANOVA with Tukey.

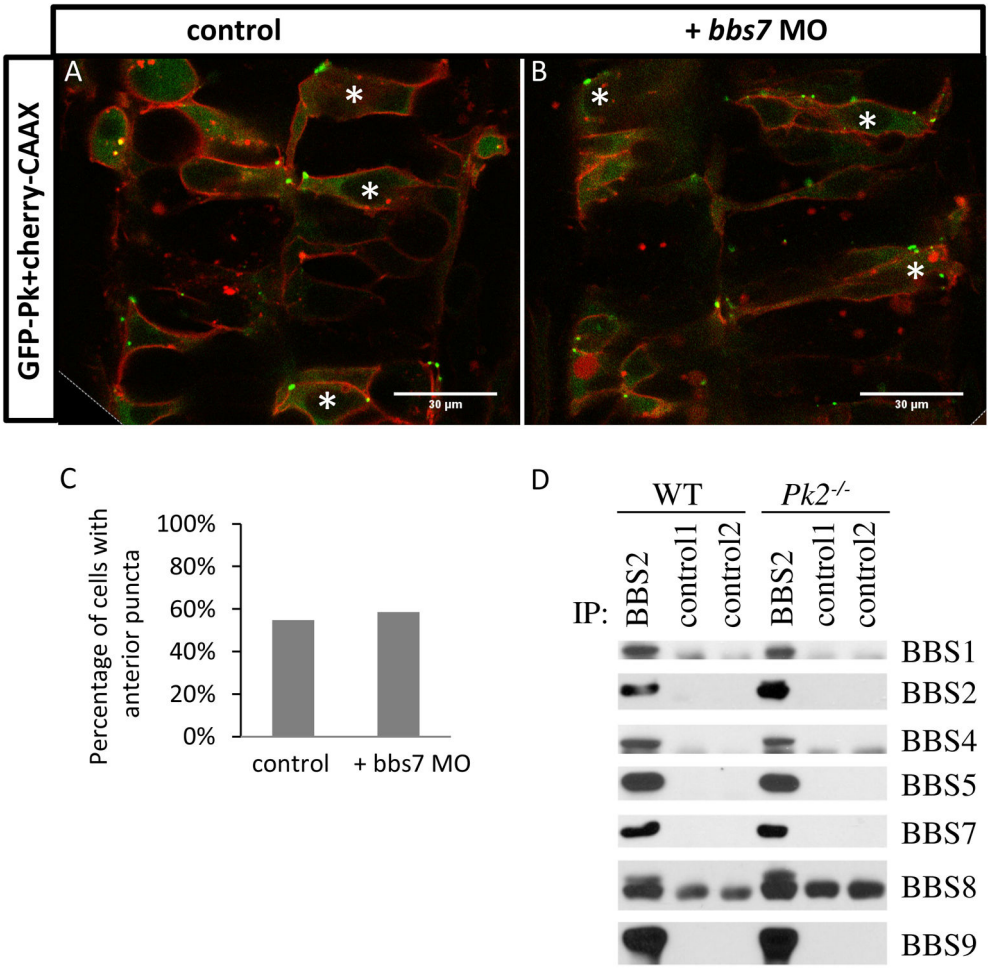

Figure 4. Normal Pk localization in *bbs7* knockown embryos and normal BBsome formation in *Pk2*$^{-/-}$ mouse tissues

A–B. GFP-Pk localization in the developing neural tube at 24hpf. A, GFP-Pk localization. B, GFP-Pk localization with *bbs7* MO injected. Asterisks mark cells with anterior GFP-Pk puncta. Anterior of the embryo is oriented to the top. Scale bars are 30μm. C. Quantification of percentage of GFP-positive cells with anterior puncta. For control, n=53; *bbs7* MO, n=41. D. Immunoprecipitation analysis demonstrates BBSome formation in *Pk2* mutants.

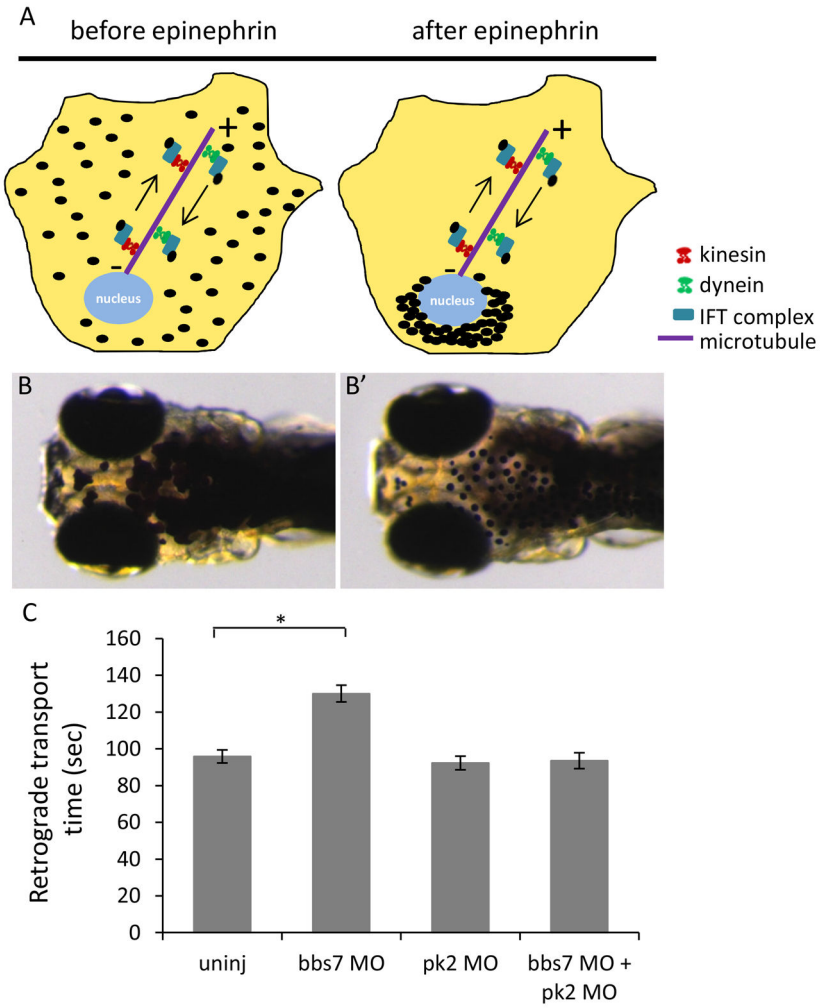

Figure 5. *pk2* knockdown suppresses the *bbs7*-related retrograde melanosome transport defect

A. Diagram of melanosome transport in melanocytes by the intracellular transport machinery. Dark-adapted are dispersed by anterograde transport while in response to light, they move to the perinuclear region by retrograde transport. B–B′. 5dpf zebrafish larva before and after epinephrine treatment. Epinephrine stimulates retrograde transport while caffeine stimulates anterograde transport. C. Graph of retrograde transport time in different groups. *bbs7* knockdown leads to a delay in the retrograde transport while *pk2* knockdown alone does not. However, the double knockdown larvae show a suppression of the retrograde transport delay. Uninj, n=50; *bbs7* MO, n=52; *pk2* MO, n=50; *bbs7* MO+*pk2* MO, n=51. Error bars are presented as standard error. *, $p<0.01$; ANOVA with Tukey.

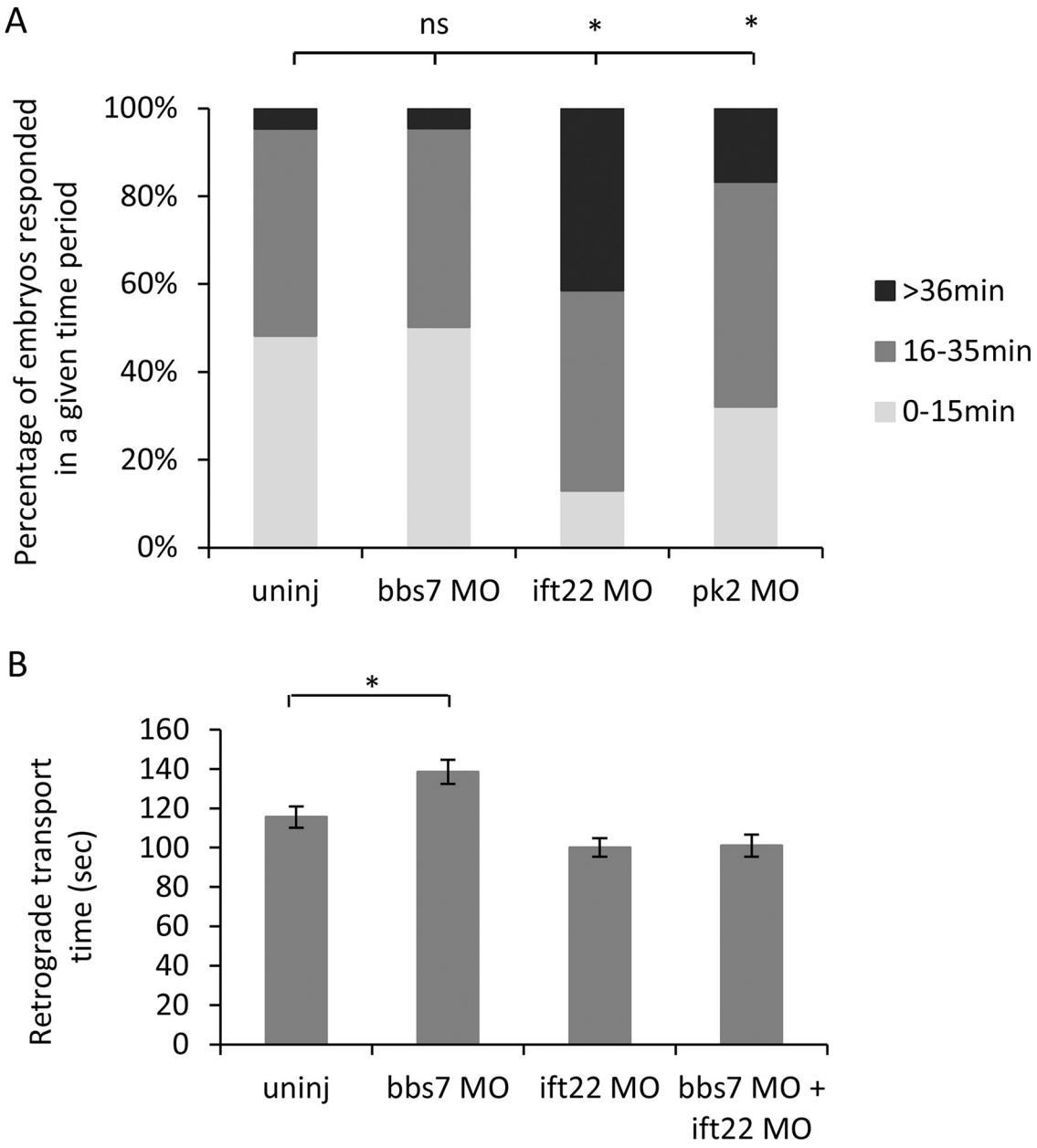

Figure 6. *pk2* knockdown shows a delay in anterograde melanosome transport

A. Graph of larva number by their anterograde melanosome transport time. Larvae are grouped by the segment of time they need to spread out their melanosome by anterograde transport. *ift22* or *pk2* knockdown but not *bbs7* knockdown leads to a delay in the anterograde transport. Uninj, n=452; *bbs7* MO, n=221; *pk2* MO, n=193; *bbs7* MO+*pk2* MO, n=162. *, p<0.01; Chi-square test. B. Graph of retrograde transport time in different groups. *ift22* knockdown alone does not show a retrograde transport delay but suppresses the *bbs7*-related retrograde transport delay. Uninj, n=67; *bbs7* MO, n=74; *ift22* MO, n=54; *bbs7* MO

+*ift22* MO, n=54. Error bars are presented as standard error. *, $p<0.01$; ANOVA with Tukey.